Article

Preparation of Crust Type Dust Suppression Gel Based on Plant Extraction Technology for *Ginkgo biloba* Leaves: Characterization, Properties, and Function Mechanism

Bo Ren [1,2], Gang Zhou [3], Mingkun Song [3,*], Bingyou Jiang [4,5], Yuannan Zheng [4,5], Tao Fan [6], Shuailong Li [3], Jing Zhao [2], Haoyang Li [4] and Hongrui Qu [3]

1 School of Emergency Management and Safety Engineering, China University of Mining and Technology (Beijing), Beijing 100083, China; renbocumt@163.com

2 State Key Laboratory for Safe Mining of Deep Coal and Environment Protection, Huainan Mining (Group) Co., Ltd., Huainan 232000, China; jzhaohfut@126.com

3 College of Safety and Environmental Engineering, Shandong University of Science and Technology, Qingdao 266590, China; zhougang@sdust.edu.cn (G.Z.); shuailong@sdust.edu.cn (S.L.); 18528029064@163.com (H.Q.)

4 School of Safety Science and Engineering, Anhui University of Science and Technology, Huainan 232001, China; cumtjiangby@163.com (B.J.); yuannanzheng@163.com (Y.Z.); 15636460305@163.com (H.L.)

5 Key Laboratory of Industrial Dust Control and Occupational Health, Ministry of Education, Anhui University of Science and Technology, Huainan 232001, China

6 Industrial Safety Research Institute, China Academy of Safety Science and Technology, Beijing 100012, China; ftanquan@126.com

* Correspondence: s18396627030@163.com

Abstract: The coal industry plays an essential role in China's economic development, and issues such as occupational health and environmental pollution caused by coal dust have attracted a great deal of attention. In accordance with the principles of environmental protection and waste management, this study used carboxymethyl ginkgo cellulose (CL) extracted and modified from *Ginkgo biloba* leaves as a matrix, and a graft copolymerized with sodium 3-allyloxy-1-hydroxy-1-propanesulfonate (AHPS) and N-isopropylacrylamide (NIPAM) monomers to prepare low-cost, environmentally friendly, and high-performance coal dust suppression (C-A-N). By optimizing fitting experimental data through three factors and two response surface analyses, the optimal dust suppression efficiency ratio was determined to be 4:8:5, and its swelling and water retention properties were analyzed. The microstructure, chemical reaction process, combustion performance and crusting property of the dust suppression gel were analyzed using Fourier-transform infrared spectroscopy (FTIR), X-ray diffraction (XRD), thermogravimetry (TG), scanning electron microscopy (SEM), cone calorimetry, and consolidation layer strength tests. Relevant experiments show that the dust suppression gel prepared in this study has the characteristics of a strong wettability and minor impacts on the calorific value of coal, as well as green and environmental protection. When the wind speed is 10 m/s, the dust suppression effect reaches 93%, and the hardness of the solidified layer reaches 39.6 KPa. This study analyzed the migration and combination of functional groups in the interaction system using molecular dynamics simulation software. The microscopic effect and mechanism between dust suppression gel and coal are revealed from a molecular point of view. The feasibility and accuracy of the molecular dynamics simulation were verified by the consistency between simulation results and experimental data. Therefore, combining the utilization of waste resources with dust suppression can have important economic and social benefits.

Keywords: *Ginkgo biloba* leaves; dust suppression materials; crust type; molecular dynamics simulation; waste utilization

1. Introduction

Coal resources are still the main form of fossil energy used in China. According to the Coal Industry Association, in 2022, China's raw coal production increased by 10.5% year-on-year [1–4]. The demand for coal is increasing, and the problems caused by coal dust pollution are becoming increasingly serious. During coal mining operations, the dust concentration can reach several hundred milligrams per cubic meter, and even if workers wear dust prevention equipment, they cannot completely block coal dust particles with a particle size of less than 0.3 µm [5–7]. Moreover, dust can pollute the environment, cause blurred vision, and easily lead to accidents. Additionally, coal dust can reduce the lifespan of mines [8,9]. As shown in Figure 1, according to public data, as of 2022, a total of 1.036 million cases of occupational diseases have been reported nationwide, including 923,000 cases of occupational pneumoconiosis, nearly half of which are cases of pneumoconiosis among coal workers [10]. Coal dust poses a serious threat to the health of workers. The long term inhalation of coal dust can lead to respiratory diseases, induce the occurrence of pneumoconiosis, and even cause death. As a chronic disease, the main pathogenesis of pneumoconiosis is due to the long-term inhalation of coal dust by workers, which gradually increases the amount of small coal dust attached to blood vessels and lung walls in the human body. The accumulation of coal dust leads to excessive pressure on the lung wall, making it impossible for the human body to breathe normally, and even worse, directly endangering human life and health.
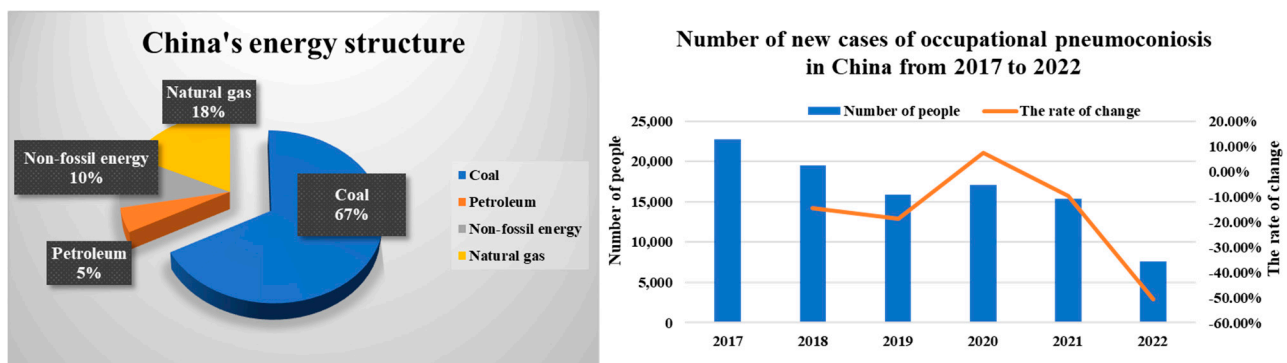

Figure 1. China's main energy structure and number of new pneumoconiosis cases in 2022.

At present, the main dust suppression method used in coal mines is spray technology [11], and the most commonly used spray technology is water spraying. However, coal dust is hydrophobic, resulting in a poor dust suppression effect and a large amount of waste, which is not in line with the current concept of green production [12,13]. Foam dust suppression technology can reduce dust emissions, but it has some shortcomings, such as poor stability, strong toxicity, high heat release, tendency to cause the spontaneous combustion of coal, etc. [14,15]. Chemical dust suppressants can moisten, bond, and agglomerate coal dust, effectively suppressing dust flying [16]. However, in the actual application process, there are still shortcomings such as poor environmental protection and high economic costs, which limit its promotion and applications [17]. Therefore, preparing an efficient, green, and safe ecological dust suppression material with water retention, wetting, and dust capture functions is essential for coal mine production [18].

Therefore, this paper analyzed and studied dust suppressants with excellent performance at home and abroad. Wei et al. [19] prepared a foam dust suppressant with carboxymethyl cellulose as an additive, and analyzed its impact on the stability of foam; Zhao et al. [20] prepared an environmentally friendly dust suppressant based on intestinal algae, using a grafting polymerization method to address the difficulties in processing Enteromorpha prolifera and the need for new environmentally friendly dust suppressants. Yu et al. [21] took inspiration from mussel adhesion protein. A large amount of gallic acid as a functional side chain was loaded onto the polyacrylic acid main chain using a

one-pot method to develop a new environmentally friendly road dust suppressant. Miguel A. Medeiros et al. [22] prepared a dust suppressant using glycerol, a byproduct of biodiesel, which has a better bonding effect than glycerol and is a good bonding dust suppressant. However, glycerol is an oily substance that can easily cause pollution in dust areas such as coal piles, which is not conducive to environmental protection. Hu et al. [23] used a biodegradable soy protein isolate as a raw material, modified it with dodecyl sodium sulfonate, and prepared dust suppressants with sodium carboxymethyl cellulose and sodium methanesilicate as additives. Zhou et al. [24] used sugarcane bagasse as raw material to prepare a wet crust dust suppressant used in coal mine production and transportation. However, currently, dust suppression materials still have limitations in terms of environmental pollution and high costs. Therefore, developing efficient, environmentally friendly, and low-cost green dust suppressants remains an important research direction for coal mine dust reduction [25,26]. In order to respond to the call from the government to build ecological environment protection and realize the integrated utilization of waste resources, a large number of ginkgo leaves were collected in autumn, and fiber samples were separated from ginkgo leaves and modified to obtain CL, which provides a matrix material for the preparation of dust suppression gel. This not only achieves the secondary utilization of waste and reduces the cost of polymer production, but also addresses interdisciplinary concepts, providing ideas for subsequent scientific research [27].

Previously, most scholars focused on the dust suppression performance of dust suppression gels, and research on the wetting effects and microscopic mechanisms of gels is limited [28]. Therefore, in this study, the C-A-N dust suppression gel was prepared using graft copolymerization with CL as the matrix, AHPS as the surfactant, NIPAM as the monomer, ammonium persulfate (APS) as the initiator, and N,N′-methylenebisacrylamide (MBA) as the crosslinking agent. The dust suppression performance of the gel was studied using the swelling degree, water retention, cone calorimetry, crusting performance, and dust suppression experiments. Scanning electron microscopy (SEM), Fourier infrared spectroscopy (FTIR) and X-ray diffraction (XRD) were used to explain the forming mechanism and microstructure of the gel, and a molecular dynamics simulation was used to explain in detail the action mechanism of the gel from a microscopic perspective. The simulation results were consistent with the experimental application, providing a new reference for the in-depth study of gel dust suppression mechanisms.

2. Experiment

2.1. Experimental Reagents

Ginkgo biloba leaves were taken from Shandong University of Science and Technology (dried to constant weight in a 60 °C drying oven, and then crushed through a 60 mesh sieve using a plant crusher). Reagents: 3-Allyloxy-2-Hydroxy-1-Propane, sodium salt (AHPS), N-Isopropylacrylamide (NIPAM), sodium persulfate (APS), Methylene-Bis-Acrylamide (MBA), hydrogen peroxide (H_2O_2), sodium chloride (NaClO), sodium hydroxide (NaOH), calcium chloride ($CaCl_2$), chloroacetic acid, ethanol absolute, and deionized water. All reagents were purchased from Qingdao Jingke Chemical Reagent Co, Ltd., Qingdao, China.

2.2. Experimental Process

2.2.1. *Ginkgo biloba* Extract Cellulose

Firstly, weigh 20 g of *Ginkgo biloba* leaves, cut the material into small pieces, place it in a 2% NaOH solution, treat it at 100 °C for 2 h, cool it to 75 °C, and add 5% H_2O_2 for 1 h [29]. Wash, filter, and dry with deionized water to obtain a mixed fiber sample. Treat the dried sample with sodium chlorite under acidic conditions at 4 °C for 5 h. Repeat the treatment three times to remove lignin and prepare a cellulose sample. Finally, treat the fiber sample with sodium hydroxide to form alkaline cellulose, which reacts with chloroacetic acid. Wash, filter, and dry the reaction product with ethanol solution to obtain carboxymethyl ginkgo cellulose.

2.2.2. C-A-N Dust Suppression Gel

The preparation process of dust suppression gel is shown in Figure 2. Firstly, accurately weigh a certain amount of CL, AHPS, and NIPAM and place them in a 300 mL beaker, and then add an appropriate amount of deionized water to the beaker. Stir the mixture until it has dissolved, and then add an appropriate amount of initiator ammonium persulfate to the flask. After stirring and thoroughly mixing, let them react for 1 h. Finally, slowly pour MAB solution into a beaker, and let the reaction proceed for 2 h. Add $CaCl_2$ solution and continue the reaction to obtain a colorless and transparent colloid. The reaction should last for 2 h, and a colorless and transparent colloid should be obtained. Then, dry the obtained colloid to a constant weight in a vacuum drying oven at 60 °C.
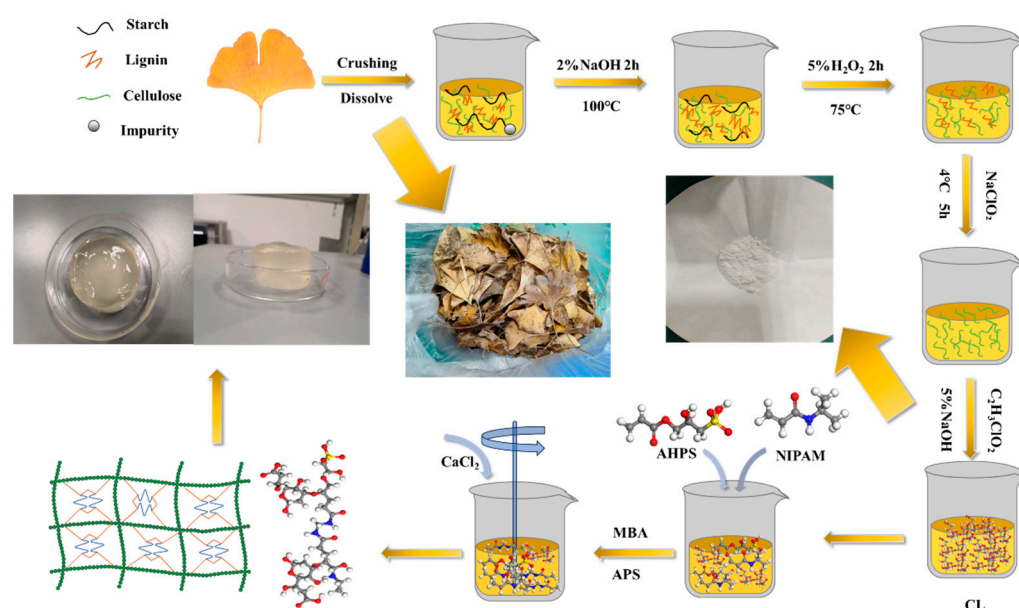

Figure 2. Preparation flow chart.

2.3. Response Surface Method Design Experiment to Determine the Optimal Ratio

Response surface methodology (RSM) is an optimization method that integrates experimental design and mathematical modeling; it can effectively reduce the number of experiments and reflect the interaction between influencing factors [30]. Design Expert 10 software was used for the experimental design and analysis of response surface methodology. First, a single-factor experiment was conducted to determine the approximate range of gel forming values, with the content of the matrix and monomer as independent variables and the swelling degree and dust suppression efficiency as response values. Response surface experiments were designed according to Box–Behnken Design (BBD) principles [31]. Then, the designs were analyzed based on experimental results. The recommended model for this experiment is a second-order model, where the quadratic term represents the interaction term, and the square term represents the surface action. The specific values are shown in Table 1. To ensure the accuracy of the experimental results, each group of experiments was repeated three times, and the average value was taken. During the preparation process, 300 mL of deionized water was used as standard.

Table 1. Experimental design of response surface method.

Level	Factor		
	NIPAM/g	AHPS/g	CL/g
Low	2	4	1
Middle	4	6	3
High	6	8	5

2.4. Gel Structure Characterization

The prepared CL, NIPAM, and the final product were dried in a vacuum drying oven at 60 °C for 24 h, and then completely ground in a mortar and passed through a 200-mesh screen using scanning electron microscopy (SEM; Apreo S HiVac, ThermoFisher, Waltham, MA, USA) and sprayed gold to observe the microscopic morphology of the sample. Fourier-transform infrared spectroscopy (FTIR; Nicolet iS50, ThermoFisher) detected the characteristic functional groups of the sample with a scanning frequency of 75 s^{-1} and a scanning range of 400–4000 cm^{-1}. X-ray diffraction spectroscopy (XRD; D8 Advance, Bruker, Billerica, MA, USA) was used to characterize the crystal structure and its variations. The scanning angle was 10–80° and the speed was 5°/min.

2.5. Gel Performance Test

2.5.1. Swelling and Water Retention Tests

Swelling degree and water retention are two of the main indicators of the structure and performance of dust suppression gel. Using the response surface method of model graphs, draw a three-dimensional response surface and contour map of the interaction between multiple factors in orthogonal experiments, intuitively reflect upon the impact of the interaction on the response value (swelling degree), and analyze the impact of each factor on swelling degree through data fitting and experimental verification.

Put C-A-N and water in the oven at different temperatures (40 °C, 60 °C, 80 °C, 100 °C, 120 °C and 140 °C), measure the change rule of their mass with time, and determine the water retention of the gel [32].

2.5.2. Dust Suppression Capability

The dust suppression efficiency reflects the ability of dust suppression materials to wrap and cover dust. As shown in Figure 3, a self-built wind dust coupling testing platform was used. Spray the prepared dust suppression gel on the surface of coal dust [33], and then spray the sample with water, $CaCl_2$, and surfactant AHPS of the same quality as the control. After ventilation for 20 min at different wind speeds (2, 4, 6, 8, and 10 m/s), the dust suppression rate was measured and compared with the control group [34]. Experimental results using dust suppression rate α are expressed as follows:

$$\alpha = 1 - \frac{(\text{Mass of coal dust before wind} - \text{Mass of coal dust after wind})}{\text{Blank dust quality}} * 100\% \quad (1)$$

Figure 3. Airflow dust coupling test platform.

2.5.3. Thermogravimetric Experiments

Dust suppression materials need to be used in different environments, so they need to have good stability. TG experiments can be used to test their thermal stability under extreme conditions. The final product was dried in a vacuum drying oven, 5–8 mg of solid powder was weighed, and the sample was placed in a high-temperature thermogravimetric analyzer (TGA/DSC 11600HT) to analyze the thermal stability of the material under a nitrogen atmosphere. In this experiment, the heating rate was set to 20 °C/min, and the temperature range was 30–600 °C.

2.5.4. Cone Calorimetry Experiments

The cone calorimetry experiment can reflect the combustion performance of materials. This article studied the combustion performance of raw coal samples and coal samples mixed with C-A-N ratio of 4:1, respectively. The thermal radiation intensity of the cone calorimeter (R-S/FTT0007) was set to 50 kW/m^2.

2.5.5. Strength of Consolidation Layer

Spray four solutions onto coal dust, dry after 24 h, observe the solidified layer, and then measure the strength of the solidified layer [35].

2.6. Analysis of C-A-N Microscopic Mechanism

Molecular dynamics simulation software was used to reveal the microscopic mechanism of gel dust suppression [36]. In this study, the force module of Materials Studio 2019 software was used, which employs a molecular mechanics method to treat atoms as spheres, and the force field describes the interaction between atoms, ions and molecules, which can describe the movement of atoms under specific thermodynamic conditions. This article adopts the optimized coal molecular structure model proposed by Zhang Zhijun [37]. The aromatic structural units of coal molecules include 2 benzene, 2 naphthalene, and 4 anthracene rings. The heteroatoms in the molecular structure of coal exist as 2 carbonyls and 1 phenolic hydroxyl, 1 pyridine and 1 pyrrole. The rectangular unit system of coal gel water is constructed. Under the COMPASS II force field, when the time step is set to 1.0 fs, the final 300 ps simulation data are used to identify the intermolecular interaction mechanism by analyzing the intermolecular interaction mode.

3. Experimental Results and Discussion

3.1. C-A-N Quadratic Response Surface Regression Analysis

Using the Box–Behnken response surface method (BBD) in response surface analysis software (Design-Expert 10) to optimize the experimental design and conduct a numerical analysis, this study selected a three-factor response surface experiment. To ensure the accuracy of the results, each experiment was repeated three times, and the average value was taken. The results are shown in Table 2. (It was found that C-A-N gel could be formed when the initiator was 0.02–0.04 g and the crosslinking agent was 0.2–0.45 g, which is only related to the forming time, and has no practical impact on the dust suppression effect. Therefore, it is not considered as an influencing factor).

Using Design-Expert 10 software for three-factor and response value Swelling quadratic response surface regression analysis, the quadratic regression equation is obtained as follows:

$$R_1 = 421.60 - 56.00A + 9.50B - 7.25C - 9.50AB - 8.50AC + 0.5BC - 64.80A^2 - 40.80B^2 - 47.30C^2 \qquad (2)$$

$$R_2 = 82.80 - 0.62A - 9.13B + 1.00C + 0.50AB - 0.25AC - 0.25BC - 1.65A^2 - 0.15B^2 + 0.60C^2 \qquad (3)$$

Table 2. Response surface analysis design and results.

Run	Facotr1	Facotr2	Facotr3	Response	Response
	A: NIPAM/g	B: AHPS/g	C: CL/g	Swelling	Dust Suppression Effect
1	4	4	5	324	92
2	4	6	3	417	83
3	4	6	3	432	82
4	4	6	3	425	84
5	6	6	1	274	80
6	6	6	5	235	82
7	4	6	3	421	83
8	6	8	3	263	90
9	2	6	5	362	84
10	4	6	3	413	82
11	2	4	3	350	73
12	2	8	3	396	90
13	4	8	1	342	92
14	6	4	3	255	71
15	2	6	1	367	81
16	4	8	5	336	93
17	4	4	1	332	73

3.2. Characterization Performance Analysis

3.2.1. Fourier-Transform Infrared Spectroscopy Analysis

Changes in functional groups before and after the reaction were analyzed by Fourier infrared spectroscopy. This is also a necessary means of determining the synthesis of materials.

From the spectrum of CL in Figure 4a, large and wide telescopic vibration peaks can be observed near 3411 cm^{-1}, 3240 cm^{-1} and 2890 cm^{-1}, indicating that CL contains a large number of intermolecular associative hydroxyl groups and intramolecular associative hydroxyl groups, and a strong telescopic vibration peak appears around 1650 cm^{-1}, which proves the existence of a carboxylic acid structure, indicating that CL was successfully prepared, and the telescopic vibration peak that appeared at 1480 cm^{-1} was attributed to primary alcohol and ether bonds. A wide telescopic vibration peak appeared near 1093 cm^{-1}, attributed to primary alcohol and hexaternary single epoxy in CL (Figure 4b). The telescopic vibration peak around 3350 cm^{-1} in the NIPAM spectrum is attributed to the secondary amine group; the telescopic vibration peak near 2883 cm^{-1} is attributed to the action of -CH$_2$-; the telescopic vibration peak of 1680 cm^{-1} is caused by the action of amide I band, C=O and N-H; and 700–1480 cm^{-1} is caused by the action of N-H and C-N in the amide II band (Figure 4c). The telescopic vibration peaks of 3417 cm^{-1}, 3260 cm^{-1} and 2890 cm^{-1} in the CL-AHPA-NIPAM spectrum were reduced by half, relative to the telescopic vibration peaks of CL, indicating that some hydroxyl groups were involved in the reaction. The telescopic vibration peaks around 1720 cm^{-1} were attributed to the amide group, indicating the successful grafting of NIPAM, and the telescopic vibration peak of 1130 cm^{-1} indicated the presence of -C-O-C-. The telescopic vibration peak of 615 cm^{-1} was attributed to the sulfonic acid group, indicating successful AHPS grafting.

3.2.2. XRD Analysis

XRD was used to characterize the crystalline form and crystallinity of the carboxymethyl *Ginkgo biloba* fiber, NIPAM, and final product. As shown in Figure 5, the diffraction peak of CL around 20° is the typical broad peak of the polymer, rather than the crystal diffraction peak, and the peak at 20–60° is the diffraction peak of NIPAM. These results show that CMC does not have a crystalline polymer structure, while NIPAM has a certain crystal structure. In the resulting product, the diffraction peak of the product at 20–60° decreases due to the absorption of the carboxyl group in CL by other molecules. However, due to the addition of AHPS and NIPAM, this product has sharper diffraction peaks in the range of 17–25°. There are many sharp diffraction peaks, indicating that grafted copolymerization occurred between

the reagents, making the structure of the product denser. It can be inferred that a chemical reaction occurred during product formation, which coincides with the conclusions reached for the FTIR analysis.
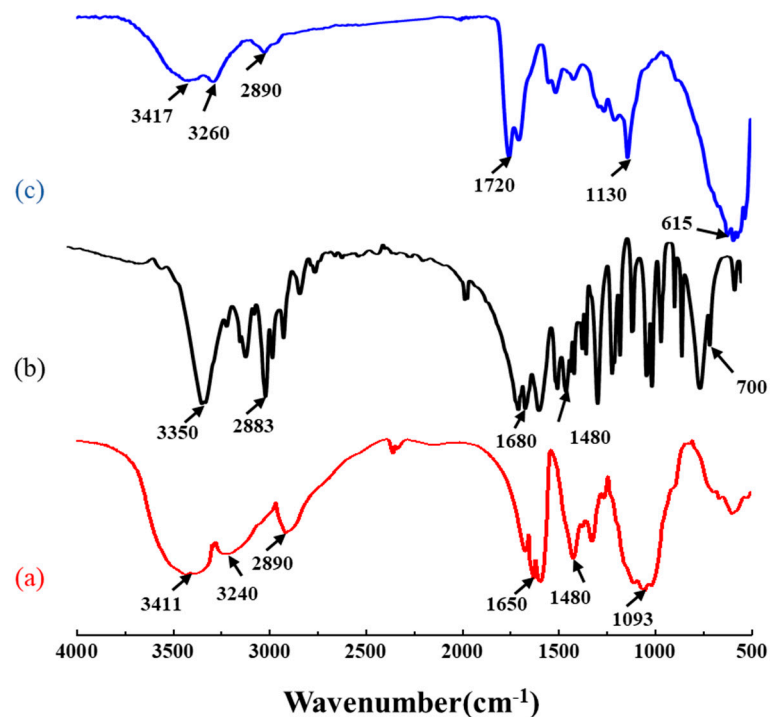
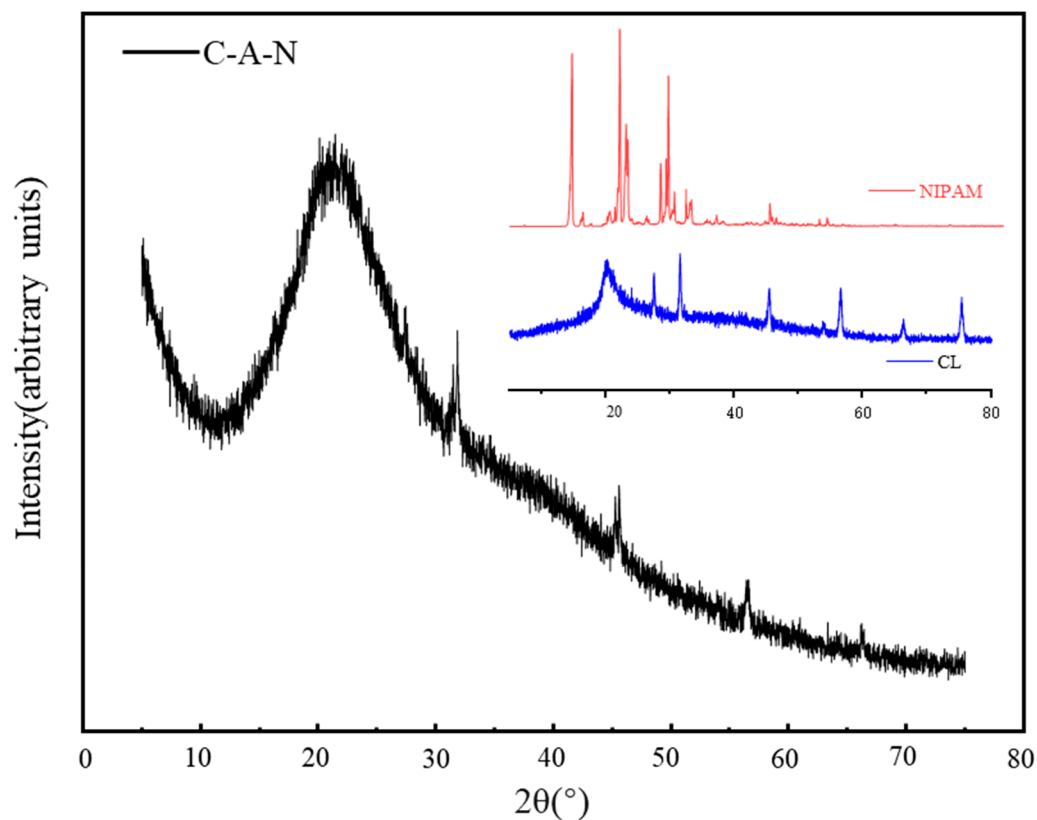**Figure 4.** Fourier infrared spectroscopy. (**a**) CL; (**b**) NIPAM; (**c**) C-A-N.

Figure 5. XRD curve.

3.2.3. SEM Analysis

From Figure 6a, it can be seen that the fragments of *Ginkgo biloba* leaves are in blocks, as the natural fibers of *Ginkgo biloba* leaves are wrapped in lignin and hemicellulose. Therefore, fibers and other matrices in *Ginkgo biloba* leaves aggregate into bundles with a diameter of approximately 200 μm. And it presents a discontinuous ceramic tile like structure. The microstructure of the sample treated with sodium hydroxide and sodium chlorite is shown in Figure 6b, with the surface attachments completely removed and the cellulose completely exposed. Presenting a disordered columnar shape, it can provide good grafting sites for monomers. The structure of the final product C-A-N is shown in Figure 6c–f. Overall, the product has good crusting and agglomeration properties, and dust suppression materials can form a consolidation layer on the surface of coal dust, producing better dust suppression effects.
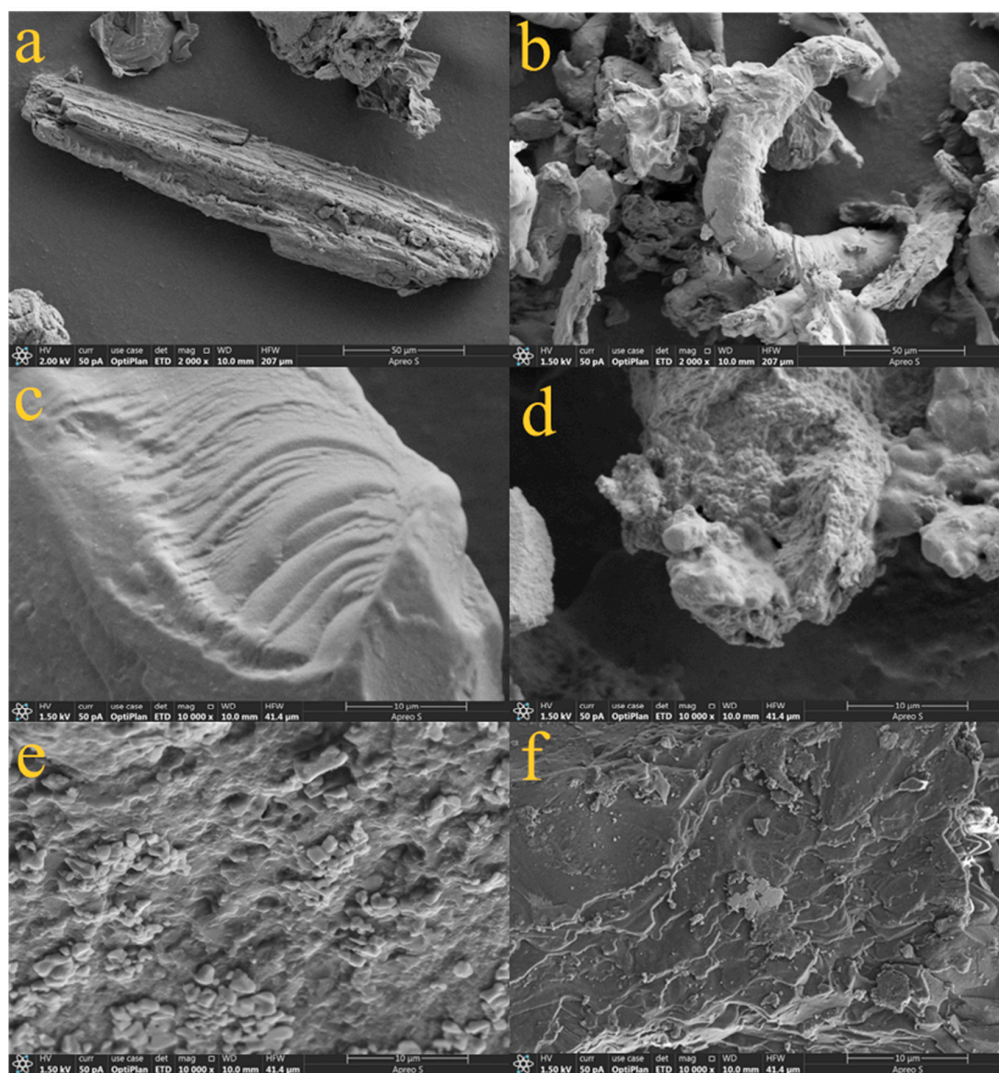

Figure 6. SEM image. (**a**) *Ginkgo biloba* fiber; (**b**) carboxymethyl *Ginkgo biloba* fiber; (**c–f**) C-A-N.

3.2.4. Synthesis Mechanism

The synthesis mechanism of the gel is shown in the figure. Under the vibration of heating and magnetic stirring, the initiator ammonium persulfate triggers the dehydrogenation of −OH in CL to form oxygen radicals, which provides a crosslinking site for subsequent AHPS and NIPAM polymerization. After the addition of AMPS and NIPAM, the C=C bond in AMPS and NIPAM is broken under the dual action of stirring and initiator. The two broken C=C bonds undergo a grafting reaction under the action of MBA to form

AHPS-NIPAM polymer [38]. CL was activated under the action of APS, and the free radicals were grafted and copolymerized under the action of MBA. MBA itself synthesized the final product with spatial network, and the molecular chains of the synthetic products were entangled with each other and arranged in an orderly manner to form a three-dimensional spatial network structure [39]. The molecular structure of the product is shown in Figure 7.
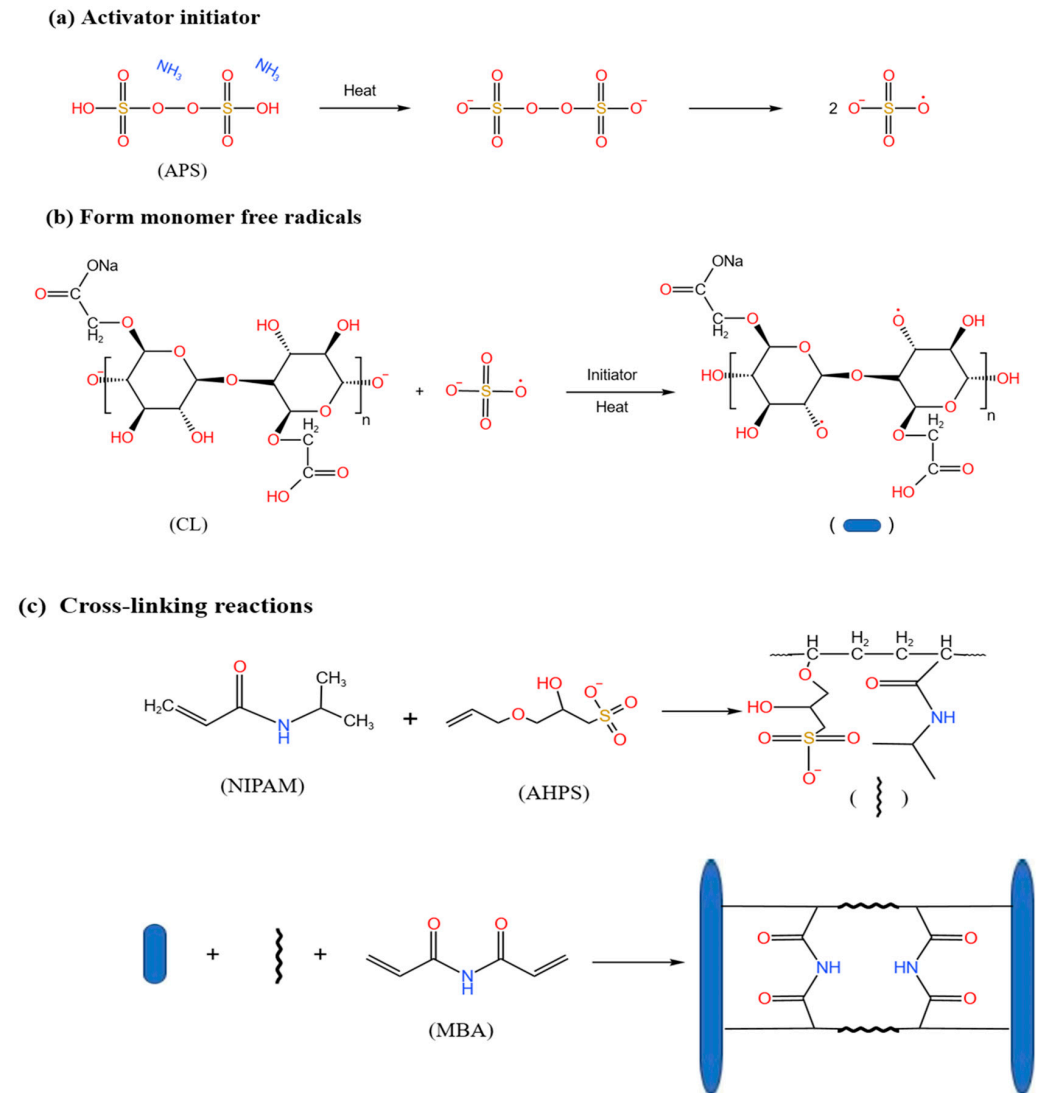

Figure 7. Diagram of synthesis mechanism.

3.3. Product Performance Test Results and Discussion

3.3.1. Dust Suppression Performance Analysis

The analysis of variance of its response surface quadratic model is shown in Table 3, and the model's independent variable significance (Prob < 0.0001) is extremely significant. The lack of fit (Prob = 0.3346) > 0.05 indicates that the mismatch term is not significant. This indicates that the fitting accuracy of the model is good, and the response surface approximation model can be used for subsequent optimization design.

The predictive decision coefficient of the model is 0.9339 > 0.8, and the adjusted decision coefficient is 0.9838 > 0.8. The difference between the predicted determination coefficient and the adjusted determination coefficient is less than 0.2, indicating that the data before and after adjustment are reasonable and consistent. Adeq accuracy represents signal-to-noise ratio (SNR). The SNR of this model is 29.452 (>4). The above results indicate that the model fits well [40].

Table 3. Analysis of variance (response value swelling degree) for the quadratic model.

Source	Sum of	F	Prob	
Model	64,786.18	108.67	<0.0001	Significant
A: NIPAM	25,088.00	378.73	<0.0001	
B: AHPS	722.00	10.90	0.0131	
C: CL	420.50	6.35	0.0398	
AB	361.00	5.45	0.0523	
AC	289.00	4.36	0.0751	
BC	1.00	0.015	0.9057	
A^2	17,680.17	266.90	<0.0001	
B^2	7009.01	105.81	<0.0001	
C^2	9420.17	142.21	<0.0001	
Lack of Fit	248.50	1.54	0.3346	Not Significant

R-Squared = 0.9929, Adj R-Squared = 0.9838, Pred R-Squared = 0.9339, Adeq Precisior = 29.452.

Figure 8a–f are the response surface analysis plots generated by fitting the quadratic regression equation $R_1 = 421.60 - 56.00\,A + 9.50\,B - 7.25\,C - 9.50\,AB - 8.50\,AC + 0.5\,BC - 64.80\,A^2 - 40.80\,B^2 - 47.30\,C^2$. The predictive determination coefficients of regression equations A and C are −56.00 and −7.25, respectively, which indicates that, with the increase in NIPAM and CL content, the swelling degree of the gel decreases. This may be because, with the increase in NIPAM and due to the hydrogen bond between the molecular chain and water, the nonpolar isopropyl group becomes hydrophobic, which significantly reduces the swelling degree. As CL increases, phase transitions occur in water, polymer chains penetrate, and different molecular chains become entangled, resulting in a decrease in swelling.
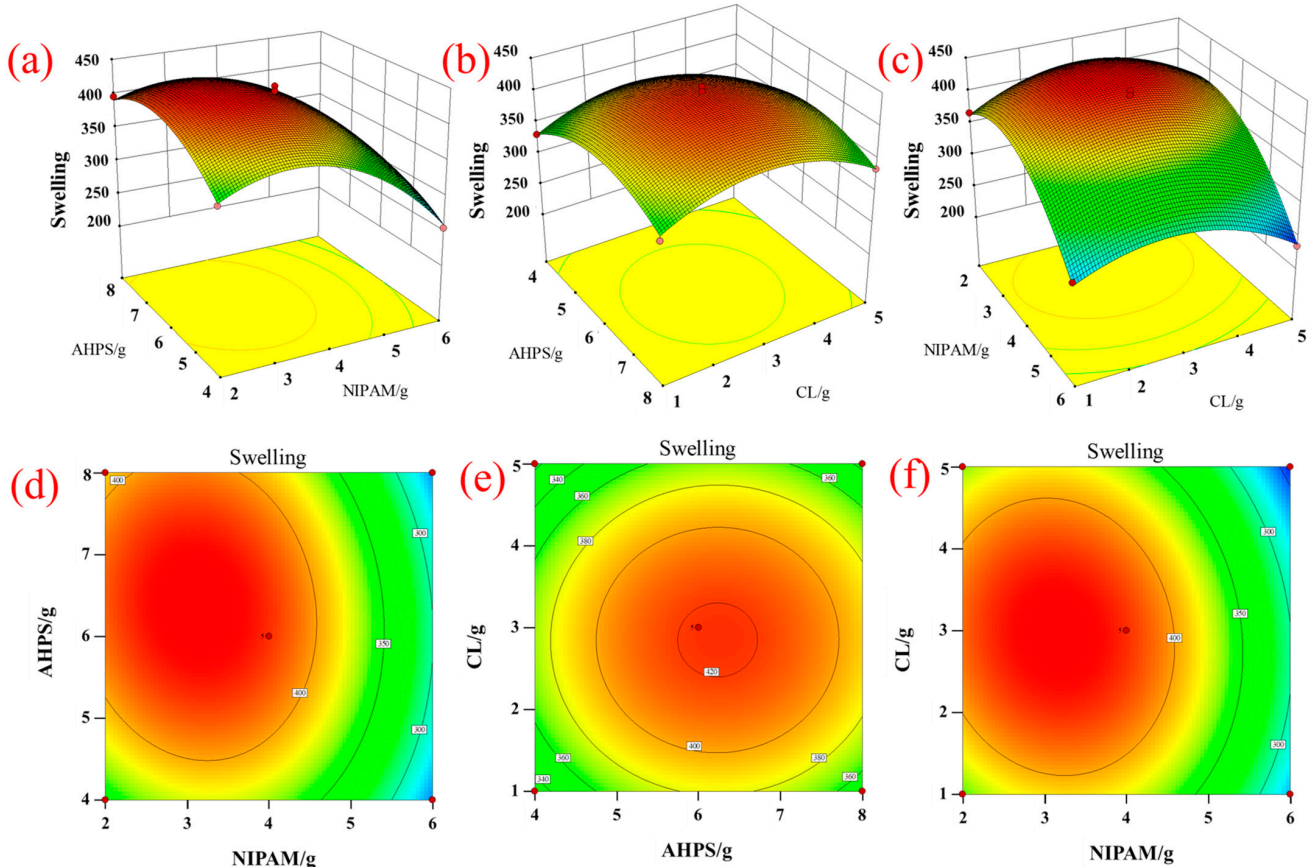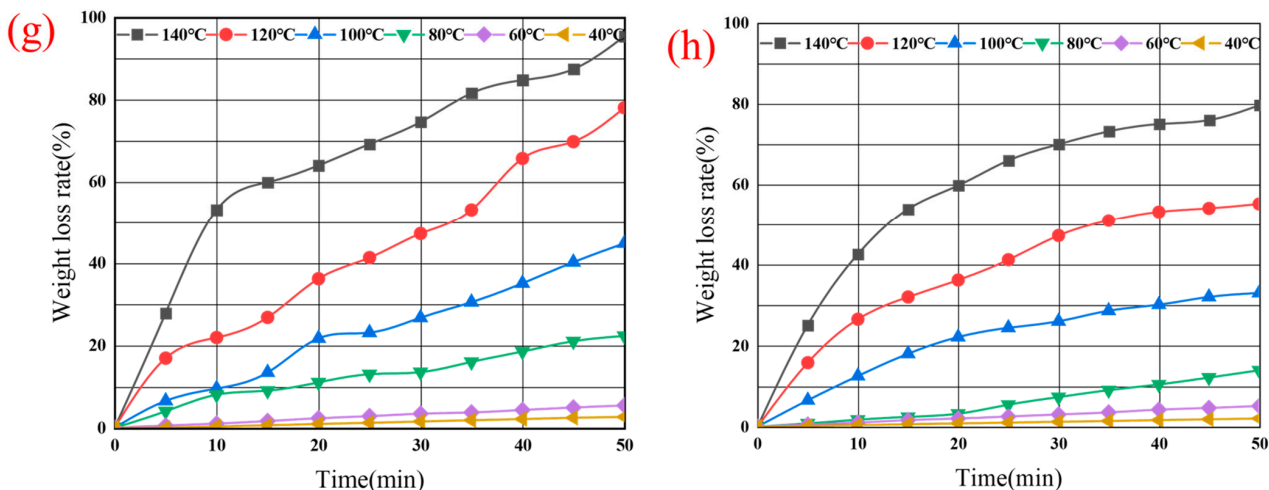

Figure 8. *Cont.*

Figure 8. Swelling and water retention analysis: (**a**–**c**) 3D surface graph of swelling degree; (**d**–**f**) contour map; (**g**,**h**) water retention analysis.

Figure 8g,h shows the change in the evolution rate of water and the gel in relation to time at different temperatures. At the same temperature, water precipitation rate gradually increases over time. When the temperature is below 60 °C, the water release rate of the gel does not significantly change with time, and the water release rate is less than 5% under conditions of continuous heating for 50 min. With the increase in experimental time, the mass loss rate of distilled water gradually accelerated, while the water release rate of gel gradually stabilized after 30 min, indicating that the gel has a good water retention performance [41].

3.3.2. Analysis of Dust Suppression Performance

The analysis of variance of its response surface quadratic model is shown in Table 4, and the model's independent variable significance (Prob < 0.0001) is extremely significant. The lack of fit (Prob = 0.7880) > 0.05 indicates that the mismatch term is not significant. This indicates that the fitting accuracy of the model is good, and the response surface approximation model can be used for subsequent optimization design.

Table 4. Analysis of variance (response value dust suppression efficiency) of the quadratic model.

Source	Sum of	F	Prob	
Model	691.51	151.50	<0.0001	Significant
A: NIPAM	3.13	6.16	0.0421	
B: AHPS	666.13	1313.49	<0.0001	
C: CL	8.00	15.77	0.0054	
AB	1.00	1.97	0.2030	
AC	0.25	0.49	0.5053	
BC	0.25	0.49	0.5053	
A^2	11.46	22.60	0.0021	
B^2	0.095	0.19	0.6786	
C^2	1.52	2.99	0.1275	
Lack of Fit	0.75	0.36	0.7880	Not Significant

R-Squared = 0.9949, Adj R-Squared = 0.9883, Pred R-Squared = 0.9764, Adeq Precisior = 40.966.

The predictive decision coefficient of the model is 0.9764 > 0.8, and the adjusted decision coefficient is 0.9883 > 0.8. The difference between the predicted determination coefficient and the adjusted determination coefficient is less than 0.2, indicating that the data before and after adjustment are reasonable and consistent. Adeq accuracy represents signal-to-noise ratio (SNR). The signal-to-noise ratio of this model is 40.966 (>4). The above results indicate that the model fits well.

Figure 9a–c show the response surface analysis generated by fitting the quadratic regression equation $R_2 = 82.80 - 0.62\,A + 9.13\,B + 1.00\,C + 0.50\,AB - 0.25\,AC - 0.25\,BC - 1.65\,A^2 - 0.15\,B^2 + 0.60\,C^2$ after spraying dust suppression materials at a wind speed of 10 m/s. According to the regression equations B and C, the predicted coefficient values are 9.13 and 1.00, respectively. This indicates that the dust suppression effect increases with the increase in AHPS and CL content. When NIPAM:AHPS:CL = 4:8:5, the material has the best dust suppression effect. This may be because AHPS is a surfactant, and as AHPS increases, the sulfonic acid group acts to better soak and adsorb coal dust. As CL increases, the material viscosity increases, increasing its adsorption effect. It is worth noting that the highest swelling degree and the best dust suppression efficiency do not appear in the same ratio. This may be because, when the swelling is too high, C-A-N adhesion decreases and the water absorption is too high, resulting in a decrease in the agglomeration and wetting effect of coal dust. Taking into account the material effect, the optimal ratio is selected as NIPAM:AHPS:CL = 4:8:5.
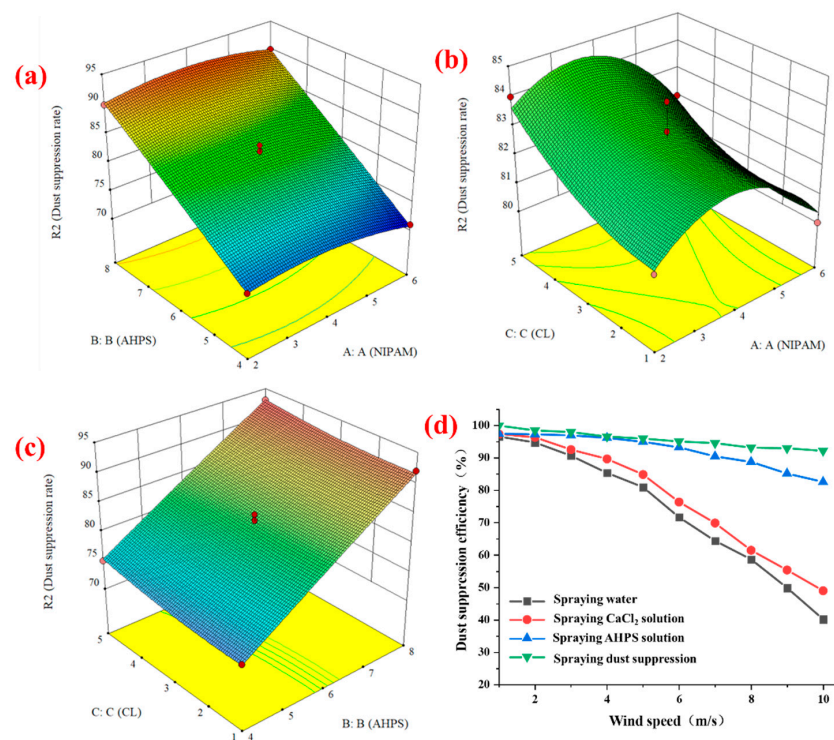

Figure 9. Analysis of dust suppression effect. (**a**–**c**) Dust suppression effect diagram at a wind speed of 10 m/s; (**d**) dust suppression effect of different materials.

Figure 9d shows the dust suppression efficiency of dust suppression materials under different wind speeds. The dust suppression effect was tested 24 h after spraying different solutions. When the wind speed reaches 6 m/s, the dust suppression rate of coal powder sprayed with dust suppression is 95%, significantly higher than that of the experimental group sprayed with water and $CaCl_2$. With the increase in wind speed, the dust suppression rate remains above 92% due to the wettability and adhesion of C-A-N, which forms a hard shell of a certain thickness on the upper part of the coal dust. When the wind speed is <5 m/s, the dust suppression efficiency of surface spraying surfactant is very high, but when the wind speed is >5 m/s, the dust suppression efficiency begins to gradually decrease. When the wind speed reaches 10 m/s, the dust suppression rate is 82.5%. When the wind speed is less than 2 m/s, the mass loss of coal dust sprayed with water and $CaCl_2$ solution is relatively small. As the wind speed increases, the dust suppression rate of water and $CaCl_2$ solution rapidly decreases. Comprehensive experiments have shown that this dust suppressant has better wind resistance and dust suppression efficiency.

3.3.3. TG-DSC of C-A-N Dust Suppression Gel

The thermal TG-DTG/DSC curve of the final product is shown in Figure 10. The TG-DTG/DSC experimental curve is divided into three main stages. In the first stage, the mass loss is very small before heating to 230 °C. Combined with the endothermic peak on the DSC curve, the mass loss during this stage is mainly caused by the volatilization of free water and crystalline water in the product, with a mass loss of approximately 8.5%. In the second stage, a significant mass loss occurred between 230 °C and 392 °C. Based on the analysis of the endothermic peak on the DSC curve, the product began to decompose, and the heat release rate of the product rapidly increased. At 300 °C, the heat release reached its maximum value, and then the heat release rate gradually slowed down. At this time, the mass loss was mainly caused by the dehydration and cracking of glycosidic and cellulose chains, with a mass loss of about 38.7%. The third stage of weightlessness is from 392 °C to 600 °C, with a mass loss of approximately 59.7%, during which the material structure is destroyed. The maximum underground temperature of the coal mine will not exceed 80 °C, while the dust suppression gel will start to decompose at 230 °C, showing good thermal stability and meeting the demand for dust suppressants in the coal mine.
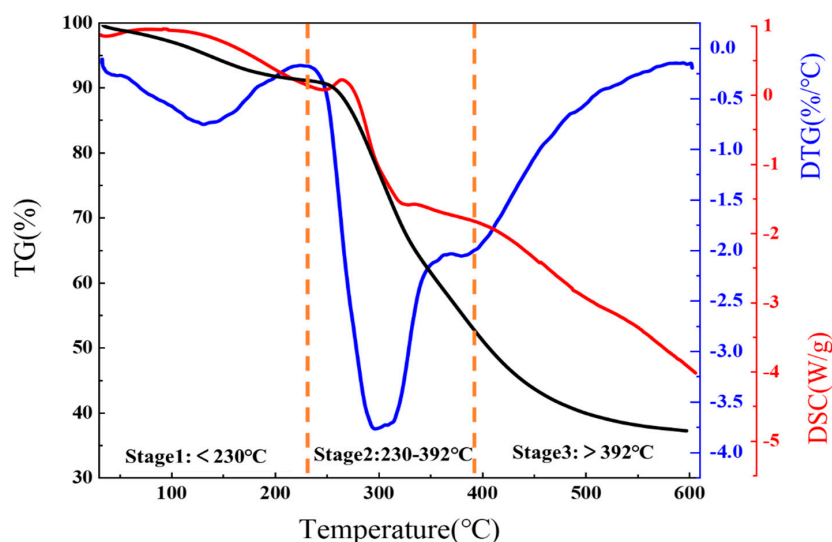

Figure 10. Thermogravimetric curve.

3.3.4. Analyzing Cone Calorimetry

This article investigates the combustion performance of raw coal samples and coal samples mixed with C-A-N. The HRR curve during the measurement period of the cone calorimetry test is shown in the figure. In the figure, it can be seen that the HRR of the two samples rapidly increased in the early stage, due to the material absorbing enough heat to reach the ignition point, causing spontaneous combustion and releasing a large amount of heat. Subsequently, the HRR curves of the two samples decreased and became stable, entering a stable combustion stage until the end.

In Figure 11a, it can be seen that the coal sample was ignited in a short period of time, reaching an exothermic peak of 53.6 Kw/m^2 around 50 s. Afterwards, the HRR curve rapidly decreased and stabilized at around 35 Kw/m^2. The mixture of the coal sample and C-A-N began to ignite and reached an exothermic peak of 35.4 Kw/m^2 at about 100 s, followed by a stable HRR of 30 Kw/m^2. Under normal circumstances, the lower the HRR, the better the flame retardant effect. It can be seen from the figure that the effective combustion heat of the mixed sample added with C-A-N has not decreased, which proves that the C-A-N gel will not reduce the calorific value of the coal and meet the needs of the mine for dust suppression.
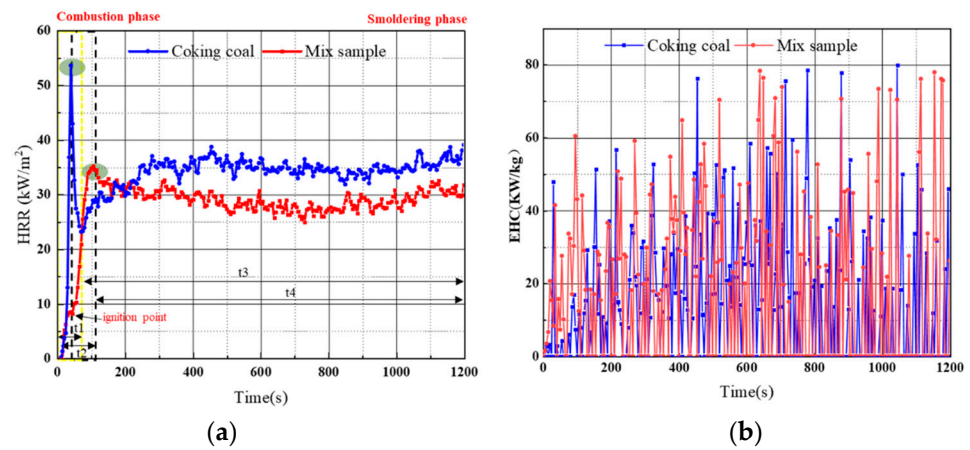
Figure 11. (**a**) HRR curve; (**b**) EHC curve.

EHC is the heat released by the combustion of combustible components in the volatile matter formed during the thermal combustion process of a material. From Figure 11b, it can be seen that there is a high fluctuation in the EHC curve of the coal sample around 100 s. Over time, the EHC curve significantly fluctuates, indicating that the combustion of the coal sample is not stable. At the initial stage of about 40 s, a peak appeared in the mixed sample, indicating that the mixed sample was ignited and began to release heat. The overall EHC curve of the mixed sample was higher than that of the coal sample, indicating that the addition of C-A-N did not affect the combustion performance of the coal sample, but rather made the combustion of the coal sample more uniform.

3.3.5. Consolidation Layer Strength

In Figure 12, the effect of spraying four solutions for 24 h can be seen. The strength of the consolidation layer with added water is essentially 0, while the strength of the consolidation layer with added dust suppression materials is as high as 39.6 Kpa. It can be seen from the physical image that the surface of the control group with added water does not form a consolidation layer, and the surface is still scattered coal dust. The curing layer on the surface with $CaCl_2$ added is a soft film and contains cracks. Surfactant solutions can be well wetted to form a thin consolidation layer, but the strength of the consolidation layer is relatively low. Dust suppression materials form a consolidated layer with a certain thickness and hardness. Overall, the dust suppression materials have the best effect.
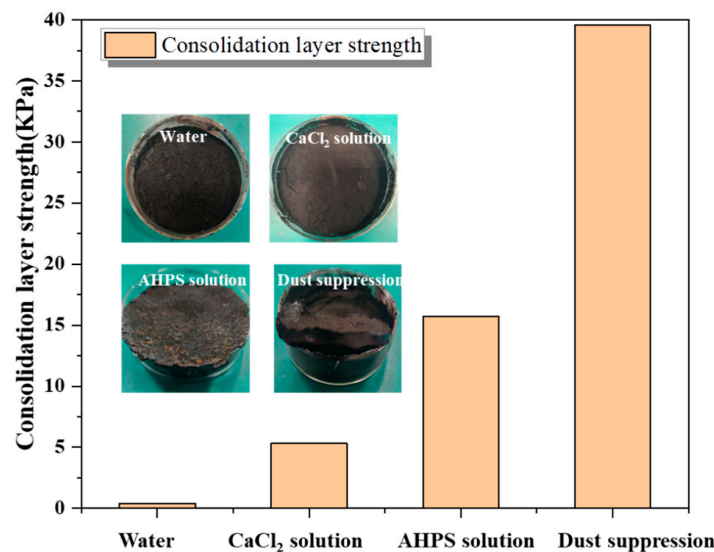

Figure 12. Consolidation layer strength of different materials.

4. Micro Function Mechanism of Dust Suppression Gel

Figure 13 shows the interaction between water molecules and gel molecules with coal molecules in the simulation process. From the figure, it can be seen that the water layer and coal seamlessly overlap at 50 Å and continue along the z-axis until 70 Å. The thickness of the adsorption layer d1 is only 20 Å. This is because the coal molecules themselves are non-polar molecules with a strong hydrophobicity, which makes their attraction to water molecules very low and repels them. However, the propane sulfonic acid in gel materials has the properties of a surfactant. After being added, it forms a network structure on the surface of coal, which enhances the wettability of coal, making the interaction between water molecules and coal stronger. At the same time, C-A-N contains a large number of −OH, −COOH groups, which reduce the surface tension of liquid through hydrogen bonding or coulomb forces [42], causing the water molecules to diffuse deeper and farther in the z-axis direction. It can be seen that the thickness d2 of the adsorption layer at the coal/water interface increases to 47 Å (23–70 Å), and the concentration of the adsorption layer is relatively high, indicating that the C-A-N gel promotes the adsorption of water molecules on the coal surface and improves the wettability of the coal surface. Through a molecular dynamics simulation, the migration of functional groups was analyzed from a microscopic perspective, and the dust suppression mechanism and wetting effect of the gel were explained. The feasibility of a molecular dynamics simulation was verified through the combination of a simulation and experiment.
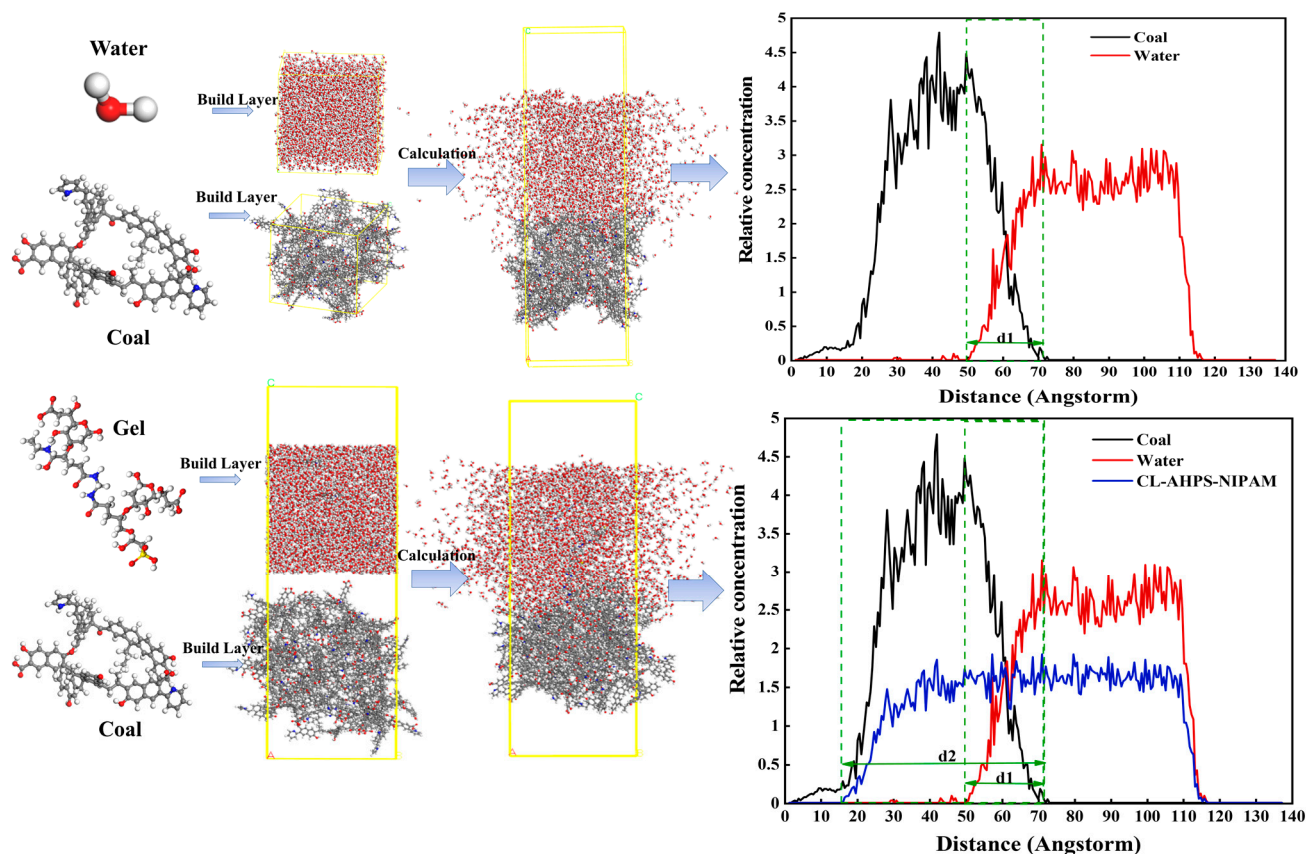

Figure 13. MS simulation.

5. Conclusions

In this study, we extracted and modified cellulose from *Ginkgo biloba* leaves and successfully prepared a dust suppression gel based on AHPS and NIPAM. It not only realized waste recycling, effectively controlled coal dust, but also complied with the national sustainable development strategy. This study analyzes the surface structure, functional

group changes, swelling degree, water retention, dust suppression effect, and consolidation layer strength of C-A-N, as well as observing the molecular migration process through molecular dynamics simulation technology. The main conclusions are as follows:

(1) Through the response surface regression analysis experiment, the fitting analysis of the best ratio of gel shows that the dust suppression effect is best when CL:AHPS:NIPAM = 4:8:5, the initiator cross-linking agent is 1:5, and the reaction temperature is 60 °C. The dust suppression effect reaches 93% when the wind speed is 10 m/s, indicating the dust suppression efficiency of the product.

(2) FT-IR, XRD, and thermogravimetry experiments proved that C-A-N was successfully prepared, and the synthesis mechanism of gel was analyzed. According to the SEM experiment, the internal structure of *Ginkgo biloba* leaves in comparison to CL and the gel was analyzed, and it was determined that the product had good thermal stability.

(3) Through cone calorimetry experiments, it was found that the calorific value of coal stabilized at 30 Kw/m^2 after adding dust suppression materials and did not decrease the calorific value of coal. The consolidation layer strength of the dust suppression material is as high as 39.6 Kpa, which proves the high crust strength of the product.

(4) Through a molecular dynamics simulation, the interaction between the dust suppressor and coal dust was further revealed from a microscopic perspective. The hydrogen bond and Van der Waals force of the functional groups in the gel system were expounded, and the dust suppression mechanism and wetting effect of the gel were explained. After adding the gel, the thickness of the adsorption layer of coal and water increased from 20 Å to 47 Å, indicating that the gel has a good wetting effect.

In this study, a dust suppression gel with a high dust suppression efficiency, high water absorption, and high consolidation strength was successfully prepared. Extracting cellulose from discarded *Ginkgo biloba* leaves has the advantages of a wide source, low cost, non-toxicity, and environmental friendliness. It can achieve the recycling and utilization of waste and effectively control coal dust, in line with the national sustainable development goals.

Author Contributions: Conceptualization, B.R., G.Z., Y.Z., J.Z. and H.L.; Methodology, M.S. and S.L.; Software, M.S. and S.L.; Validation, M.S. and T.F.; Formal analysis, M.S.; Investigation, M.S. and B.J.; Resources, G.Z.; Data curation, M.S.; Writing—original draft, M.S.; Visualization, H.Q.; Project administration, G.Z.; Funding acquisition, G.Z. All authors have read and agreed to the published version of the manuscript.

Data Availability Statement: The data presented in this study are available on request from the corresponding author.

Conflicts of Interest: Authors Bo Ren and Jing Zhao are employed by the company State Key Laboratory for Safe Mining of Deep Coal and Environment Protection, Huainan Mining (Group) Co., Ltd. The remaining authors declare that the research was conducted in the absence of any commercial or financial relationships that could be construed as potential conflicts of interest.

References

1. Zhang, H.H.; Nie, W.; Yan, J.Y.; Bao, Q.; Wang, H.K.; Jin, H.; Peng, H.T.; Chen, D.W.; Liu, Z.Q.; Liu, Q. Preparation and performance study of a novel polymeric spraying dust suppression agent with enhanced wetting and coagulation properties for coal mine. *Powder Technol.* **2020**, *364*, 901–914. [CrossRef]

2. Yang, X.H.; Yu, H.M.; Wang, Y.H.; Cheng, W.M. Investigation of dust pollution control rules in tunnel excavation based on modularized airflow diverging system. *Build. Environ.* **2022**, *221*, 109356. [CrossRef]

3. Wang, P.F.; Shi, Y.J.; Zhang, L.Y.; Li, Y.J. Effect of structural parameters on atomization characteristics and dust reduction performance of internal-mixing air-assisted atomizer nozzle. *Process Saf. Environ.* **2019**, *128*, 316–328. [CrossRef]

4.   Fabiano, B.; Currò, F.; Reverberi, A.P.; Palazzi, E. Coal dust emissions: From environmental control to risk minimization by underground transport. An applicative case-study. *Process Saf. Environ.* **2014**, *92*, 150–159. [CrossRef]

5.   Luo, Q.M.; Huang, L.P.; Xue, X.Y.; Chen, Z.S.; Zhou, F.B.; Wei, L.H.; Hua, J.M. Occupational health risk assessment based on dust exposure during earthwork construction. *J. Build. Eng.* **2021**, *44*, 103186. [CrossRef]

6.   Zhang, R.; Liu, S.M.; Zheng, S.Y. Characterization of nano-to-micron sized respirable coal dust: Particle surface alteration and the health impact. *J. Hazard. Mater.* **2021**, *413*, 125447. [CrossRef]

7.   Nie, W.; Niu, W.J.; Bao, Q.; Yuan, M.Y.; Zhou, W.W.; Hua, Y.; Yu, F.N.; Liu, C.Y.; Zhang, S.B.; Zhang, X. Study on the combined dust suppression effect of sodium alginate and sodium fatty acid methyl ester sulfonate. *Adv. Powder Technol.* **2022**, *33*, 103827. [CrossRef]

8.   Lööw, J.; Nygren, M. Initiatives for increased safety in the Swedish mining industry: Studying 30 years of improved accident rates. *Safety Sci.* **2019**, *117*, 437–446. [CrossRef]

9.   Wei, L.J.; Su, M.Q.; Wang, K.; Chen, S.N.; Ju, Y.; Zhao, S.J.; Kong, X.B.; Chu, Y.; Wang, L.X. Suppression effects of ABC powder on explosion characteristics of hybrid CH/polyethylene dust. *Fuel* **2022**, *310*, 122159. [CrossRef]

10. Dong, H.; Yu, H.M.; Xu, R.X.; Cheng, W.M.; Ye, Y.X.; Xie, S. Application and characterization of new polymer dust suppression foam in coal mine and tunnel construction space. *Constr. Build. Mater.* **2023**, *397*, 132378. [CrossRef]

11. Niu, W.J.; Nie, W.; Yuan, M.Y.; Bao, Q.; Zhou, W.W.; Yan, J.Y.; Yu, F.N.; Liu, C.Y.; Sun, N.; Xue, Q.Q. Study of the microscopic mechanism of lauryl glucoside wetting coal dust: Environmental pollution prevention and control. *J. Hazard. Mater.* **2021**, *412*, 125223. [CrossRef]

12. Shi, G.Q.; Han, C.; Wang, Y.M.; Wang, H.T. Experimental study on synergistic wetting of a coal dust with dust suppressant compounded with noncationic surfactants and its mechanism analysis. *Powder Technol.* **2019**, *356*, 1077–1086. [CrossRef]

13. Xu, R.X.; Yu, H.M.; Dong, H.; Ye, Y.X.; Xie, S. Preparation and properties of modified starch-based low viscosity and high consolidation foam dust suppressant. *J. Hazard. Mater.* **2023**, *452*, 131238. [CrossRef] [PubMed]

14. Wang, H.T.; Chen, X.Y.; Xie, Y.; Wei, X.B.; Liu, W.V. Experimental study on improving performance of dust-suppression foam by magnetization. *Colloids Surf. A* **2019**, *577*, 370–377. [CrossRef]

15. Zhang, Q.; Wang, H.T.; Han, H.; Zhao, X.; Li, X.J.; Wang, Y.X. Experimental study on improving salt resistance of dust suppressing foam with polymers. *Fuel* **2023**, *353*, 129036. [CrossRef]

16. Cheng, J.W.; Zheng, X.R.; Lei, Y.D.; Luo, W.; Wang, Y.; Borowski, M.; Li, X.C.; Song, W.T.; Wang, Z.; Wang, K. A compound binder of coal dust wetting and suppression for coal pile. *Process Saf. Environ.* **2021**, *147*, 92–102. [CrossRef]

17. Wu, M.Y.; Hu, X.M.; Zhang, Q.; Lu, W.; Zhao, Y.Y.; He, Z.L. Study on preparation and properties of environmentally-friendly dust suppressant with semi-interpenetrating network structure. *J. Clean. Prod.* **2020**, *259*, 120870.

18. Yang, X.; Qiao, Z.J.; Miao, Y.Z.; Tian, W.L.; Qing, L.B.; Jiang, L. Self-healing performance of rubber modified asphalt mixtures with microcapsules. *J. Shandong Univ. Sci. Technol. (Nat. Sci.)* **2023**, *42*, 68–76.

19. Wei, X.B.; Wang, H.T.; Xie, Y.; Du, Y.H. An experimental investigation on the effect of carboxymethyl cellulose on morphological characteristics of dust-suppression foam and its mechanism exploration. *Process Saf. Environ.* **2020**, *135*, 126–134. [CrossRef]

20. Zhao, Z.D.; Zhao, Y.Y.; Hu, X.M.; Cheng, W.M.; Hou, J.Y.; Song, C.Y. Preparation and performance analysis of enteromorpha-based environmentally friendly dust suppressant. *Powder Technol.* **2021**, *393*, 323–332. [CrossRef]

21. Yu, X.X.; Zhao, Y.Y.; Feng, Y.; Hu, X.M.; Liu, J.D.; Wang, X.W.; Wu, M.Y.; Dong, H.; Liang, Y.T.; Wang, W.; et al. Synthesis and performance characterization of a road coal dust suppressant with excellent consolidation, adhesion, and weather resistance. *Colloids Surf. A* **2022**, *639*, 128334. [CrossRef]

22. Joshi, G.; Naithani, S.; Varshney, V.K.; Bisht, S.S.; Rana, V.; Gupta, P.K. Synthesis and characterization of carboxymethyl cellulose from office waste paper: A greener approach towards waste management. *Waste Manag.* **2015**, *38*, 33–40. [CrossRef] [PubMed]

23. Jin, H.; Nie, W.; Zhang, Y.S.; Wang, H.K.; Zhang, H.H.; Bao, Q.; Yan, J.Y. Development of Environmental Friendly Dust Suppressant Based on the Modification of Soybean Protein Isolate. *Processes* **2019**, *7*, 165. [CrossRef]

24. Zhou, G.; Xu, Y.X.; Wang, Q.; Jiang, B.Y.; Ren, B.; Zhang, X.Y.; Yi, L.X. Wetting-consolidation type dust suppressant based on sugarcane bagasse as an environmental material: Preparation, characterization and dust suppression mechanism. *J. Environ. Manag.* **2023**, *330*, 117097. [CrossRef]

25. Lu, Z.; Lei, Z.; Zafar, M.N. Synthesis and performance characterization of an efficient environmental-friendly Sapindus mukorossi saponins based hybrid coal dust suppressant. *J. Clean. Prod.* **2021**, *306*, 127261. [CrossRef]

26. Zhu, Y.Y.; Cui, Y.M.; Shan, Z.H.; Dai, R.; Shi, L.; Chen, H. Fabrication and characterization of a multi-functional and environmentally-friendly starch/organo-bentonite composite liquid dust suppressant. *Powder Technol.* **2021**, *391*, 532–543. [CrossRef]

27. Medeiros, M.A.; Leite, C.M.M.; Lago, R.M. Use of glycerol by-product of biodiesel to produce an efficient dust suppressant. *Chem. Eng. J.* **2012**, *180*, 364–369. [CrossRef]

28. Gao, Z.J.; Ding, Z.Q.; Liu, J.T.; Wang, Z.Y.; Wang, S.; Liu, W.Y. Study on water distribution and migration characteristics of inverted saturated zone and unsaturated zone beneath river. *J. Shandong Univ. Sci. Technol. (Nat. Sci.)* **2023**, *42*, 1–10.

29. Waghmare, N.K.; Khan, S. Extraction and Characterization of Nano-cellulose Fibrils from Indian Sugarcane Bagasse-an Agro Waste. *J. Nat. Fibers* **2022**, *19*, 6230–6238. [CrossRef]

30. Li, Y.Y.; Xiao, G.Q.; Li, F.Z.; Chen, C.Y.; Chen, C.L.; Li, R.L.; Zou, R.; Zhang, M. Response Surface Analysis (RSA) optimization of temperature-resistant gel foam fabrication and performance evaluation. *Colloids Surf. A* **2022**, *655*, 130260. [CrossRef]

31. Xue, D.; Hu, X.M.; Sun, G.Z.; Wang, K.; Liu, T.Y.; Wang, J.Q.; Wang, F.S. A study on a Janus-type composite solidified foam and its characteristics for preventing and controlling spontaneous combustion of coal. *Energy* **2023**, *275*, 127433. [CrossRef]

32. Zhang, H.H.; Nie, W.; Wang, H.K.; Bao, Q.; Jin, H.; Liu, Y.H. Preparation and experimental dust suppression performance characterization of a novel guar gum-modification-based environmentally-friendly degradable dust suppressant. *Powder Technol.* **2018**, *339*, 314–325. [CrossRef]

33. Liu, J.G.; Wang, T.Y.; Jin, L.Z.; Li, G.; Wang, S.; Wei, Y.X.; Ou, S.N.; Wang, Y.P.; Xu, J.G.; Lin, M.L.; et al. Suppression Characteristics and Mechanism of Molasses Solution on Coal Dust: A Low-Cost and Environment-Friendly Suppression Method in Coal Mines. *Int. J. Environ. Res. Public Health* **2022**, *19*, 16472. [CrossRef]

34. Zhou, L.; Yang, S.Y.; Hu, B.; Yuan, Z.L.; Wu, H.; Yang, L.J. Evaluating of the performance of a composite wetting dust suppressant on lignite dust. *Powder Technol.* **2018**, *339*, 882–893. [CrossRef]

35. Yan, J.Y.; Nie, W.; Zhang, H.H.; Xiu, Z.H.; Bao, Q.; Wang, H.K.; Jin, H.; Zhou, W.J. Synthesis and performance measurement of a modified polymer dust suppressant. *Adv. Powder Technol.* **2020**, *31*, 792–803. [CrossRef]

36. Zhang, R.; Xing, Y.W.; Xia, Y.C.; Guo, F.Y.; Ding, S.H.; Tan, J.L.; Che, T.; Meng, F.C.; Gui, X.H. Synergistic Adsorption Mechanism of Anionic and Cationic Surfactant Mixtures on Low-Rank Coal Flotation. *ACS Omega* **2020**, *5*, 20630–20637. [CrossRef]

37. Zhang, Z.J.; Wang, L.; Li, H. Study on model construction and optimization of molecular structure. *Coal Sci. Technol.* **2021**, *49*, 245–253. [CrossRef]

38. Bao, Q.; Nie, W.; Liu, C.Q.; Zhang, H.H.; Wang, H.K.; Jin, H.; Yan, J.Y.; Liu, Q. The preparation of a novel hydrogel based on crosslinked polymers for suppressing coal dusts. *J. Clean. Prod.* **2020**, *249*, 119343. [CrossRef]

39. Gao, M.Z.; Li, H.M.; Zhao, Y.; Liu, Y.T.; Zhou, W.Q.; Li, L.M.; Xie, J.; Deng, J. Mechanism of micro-wetting of highly hydrophobic coal dust in underground mining and new wetting agent development. *Int. J. Min. Sci. Technol.* **2023**, *33*, 31–46. [CrossRef]

40. Fan, Y.J.; Zhao, Y.Y.; Hu, X.M.; Cheng, W.M.; Tang, X.L.; Zhu, S.C.; Song, C.Y. Material optimization of microbial dust suppressant nutrient solution based on response surface curve. *Powder Technol.* **2021**, *385*, 29–36. [CrossRef]

41. Wang, Y.; Du, C.F.; Cui, M.M. Formulation Development and Performance Characterization of Ecological Dust Suppressant for Road Surfaces in Cities. *Appl. Sci.* **2021**, *11*, 10466. [CrossRef]

42. Li, W.F.; Wang, H.N.; Li, X.; Liang, Y.N.; Wang, Y.T.; Zhang, H.J. Effect of mixed cationic/anionic surfactants on the low-rank coal wettability by an experimental and molecular dynamics simulation. *Fuel* **2021**, *289*, 119886. [CrossRef]